ACS APPLIED POLYMER MATERIALS

pubs.acs.org/acsapm

Article

Self-Healing of Electrical Damage in Microphase-Separated Polyurethane Elastomers with Robust Dielectric Strength Utilizing Dynamic Hydrogen Bonding Networks

Tian Tan,* Wah Hoon Siew, Lu Han, Martin Given, Christina McKendry, John Liggat, Qi Li,* and Jinliang He*

Cite This: ACS Appl. Polym. Mater. 2023, 5, 7132−7143

Read Online

ACCESS | Metrics & More | Article Recommendations | Supporting Information

ABSTRACT: Polymer dielectrics are predominantly used as primary insulating materials in various electrical and electronic systems. Recently, self-healing dielectrics have been designed to heal microdamage in polymers to repair discharge channels and restore their critical insulating properties. However, the low dielectric strength of extrinsic self-healing polymers is a critical disadvantage in preventing them from practical application. In this work, we designed and implemented an insulating robust self-healing polyurethane (PU) utilizing a microphase-separating structure with a shape memory effect. The microphase separation structure in the PUs allows hard segments (HSs) to provide high dielectric strength while achieving self-healing through the soft segments (SSs) with high flowability. The analysis of dielectric relaxation behavior and quantum chemical calculations in combination indicated that the energy barrier at the interface of SS and HS is the key factor in improving the dielectric strength of polyurethanes. Observations from three-dimensional computed micro-X-ray tomography and optical microscopy showed that the PU developed can fully heal the damaged area under moderate thermal stimulation while restoring its electrical performance. The calculation of conformational entropy and the verification of the reversibility of hydrogen bonds further illustrated the reason for efficient self-healing capability of the designed PU. This work opened up opportunities for reliable applications of self-healing dielectrics in electrical and electronic apparatus.

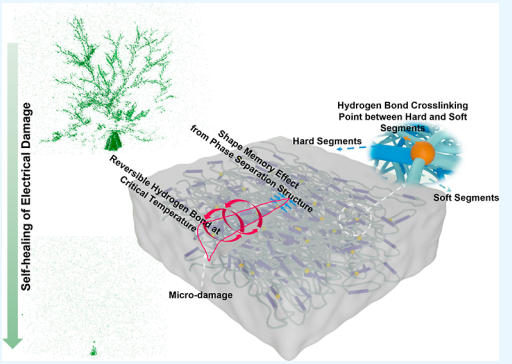

KEYWORDS: *self-healing, polyurethane elastomers, shape memory, microphase separation, electrical damage*

INTRODUCTION

With the rapid development of the global energy industry, the demand for electrical and electronic apparatus with more reliable performance and longer lifetimes becomes more emergent.[1−3] Polymeric dielectric materials play a key role in power devices, whose stability and durability largely determine the service life of the equipment.[4−6] Traditional dielectric materials are designed to be as robust as possible by employing voltage stabilizers or nanofillers to prevent equipment failure faced with increasingly complicated application scenarios.[7,8] However, in the process of manufacture, transportation, and operation, polymer materials are inevitably subjected to long-term electrical, thermal, and mechanical stress, which may cause microdefects in the materials.[9] In electrical fields, microdefects tend to induce electrical distortion, causing continuous partial discharges, which result in electron avalanches and dendritic microchannels growing progressively in the polymer.[10] Deterioration accumulation in solid dielectrics continuously operating under a harsh environment will inevitably give rise to a catastrophic failure.[11]

Recently, some self-healing polymeric dielectrics inspired by living organisms have been developed to conquer these challenges.[12] Self-healing dielectrics can heal the internal damage and recover the degraded properties to extend the lifetimes of materials. The last breakthroughs involved the utilization of superparamagnetic nanoparticles to fix the electrical tree channels of polymers and the introduction of microcapsules containing corresponding healing agents into traditional insulating polymers, such as cross-linked polyethylene and epoxy resin.[13−17] The above methods used an extrinsic self-healing mechanism; that is, the self-healing process relies on microcapsules or pipes containing a healing agent to achieve recovery. The microcracks formed in the material will result in microcapsule rupturing, thereby releasing

Received: May 31, 2023
Accepted: August 14, 2023
Published: August 22, 2023

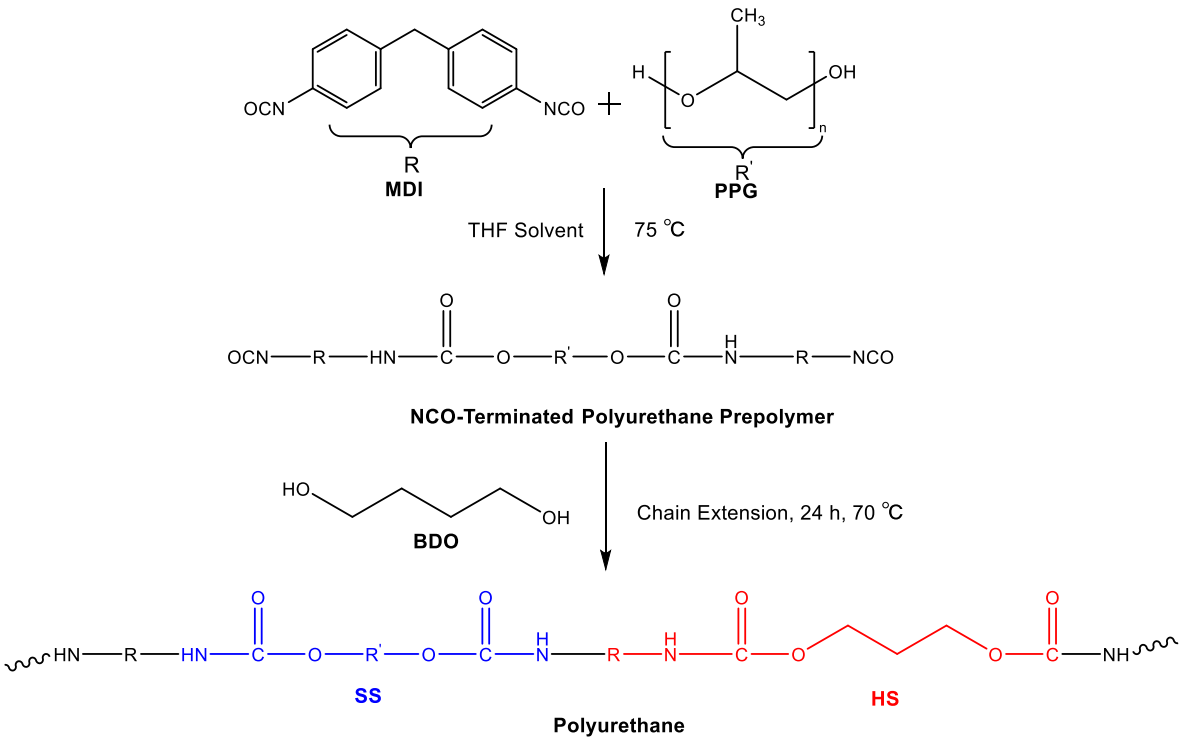

Figure 1. Synthesis route of PUs.

the healing agent, and crack healing will take place.[18] It cannot be ignored that extrinsic self-healing is not unlimited and depends on the continued availability of healing agents.[19] In contrast, intrinsic self-healing systems can heal multiple times through inherent reversible bonds or supramolecular interactions.[20] The repeatability and universality of intrinsic self-healing methods give them a better application prospect than extrinsic self-healing methods. However, it is inevitable that either the introduction of extrinsic microcapsules or intrinsic polar reversible bonds reported previously will lead to a compromise of critical properties of the polymers.[21]

Polyurethane elastomers (PUs) are typical multiblock copolymers that consist of alternating hard segments (HSs) and soft segments (SSs). Very often, the flexible and long SSs are made from long chains of polyesters or polyethers, and the polar and rigid HSs consist of diisocyanate and chain extenders.[22] The thermodynamic incompatibility of the HSs and SSs results in a unique microphase-separated structure of the PU at mesoscopic length scales.[23] The HSs form physical cross-links arising from polar interactions, hydrogen bonding, and potential crystallization in the hard domain, while the SSs form a reversible phase because of the molecular motion in the "rubbery" state.[24] Resulting from the specific microphase separation structure, PUs offer a series of versatile and seemingly contradictory properties, such as superior mechanical strength while retaining great elasticity and even the shape memory effect, which make PUs interesting for various applications, including biomedical, automotive, and electronic industries.[25−27] Additionally, PUs can be processed as typical recyclable thermoplastics due to the thermal restoration of their allophanate groups or the reversible cross-linking network composed of hydrogen bonds.[28,29] Extensive research confirms that PUs are widely suitable polymers for achieving intrinsic self-healing systems, which are benefited from their numerous synthetic raw materials and good mobility of SSs.[30] The segmented block copolymer structure of PUs may be a reliable solution to the low dielectric strength of the existing self-healing dielectrics.

In this work, we developed and prepared a series of PUs with different contents and structures of SSs and HSs. Fourier transform infrared (FTIR) spectrometry and atomic force microscopy (AFM) were first used to analyze the hydrogen bonding network and microphase separating structure of PU samples. The electrical strength of the PU samples was then tested and used as a performance screening indicator. Meanwhile, the charge transport mechanism of the PU samples was analyzed by combining the laboratory experiments and simulation calculations. Subsequently, the self-healing performance of the screened PU samples for electrical damage was examined both macroscopically and microscopically with the recovery of electrical properties investigated. Finally, the self-healing mechanism of PUs was analyzed and discussed in terms of the reversible hydrogen bonding network and shape memory effect. This paper introduces a pioneering concept and a prospect for developing self-healing dielectric polymers with excellent dielectric strength.

EXPERIMENTAL SETUP

Materials. PUs were synthesized using two bifunctional polypropylene glycol (PPG) with different molecular weights, Arcol 1004 (MW = 450, obtained from Covestro), Lupranol 1100 (MW = 1100, obtained from BASF), 4,4′-methylene diphenyl diisocyanate (MDI, obtained from Covestro), and 1,4-butanediol (BDO, obtained from Sigma-Aldrich). The PPG oligomers and BDO were dried and degassed under vacuum in a flask at 70 °C for 24 h. All PUs were prepared by a typical two-step polymerization in a three-necked round-bottom flask equipped with an anchor-type propeller stirrer, a funnel, and a nitrogen inlet. In the first step, prepolymerization, an NCO-terminated prepolymer, was prepared by carefully adding MDI to the flask containing the appropriate dried PPG at 70 °C, while keeping the rotational speed at 400 rpm for 2 h. In the second step,

https://doi.org/10.1021/acsapm.3c01155
ACS Appl. Polym. Mater. 2023, 5, 7132−7143

Table 1. Chemical Composition of Model PUs

sample code	molecular weight of PPG	isocyanate	chain extender	molar ratio (isocyanate/PPG/chain extender)	wt % of HS (%)
PU1	450	MDI		2.1:2.1:0	
PU2	450	MDI	BDO	2.1:2:0.1	35
PU3	450	MDI	BDO	2.2:1:1.2	55
PU4	1100	MDI	BDO	2.2:1:1.2	35

$$\text{wt \% of HS} = \frac{\text{weight}_{BDO} + \text{weight}_{MDI}}{\text{weight}_{BDO} + \text{weight}_{PPG} + \text{weight}_{MDI}} \times 100\% \ (\text{weight}_{BDO} \neq 0)$$

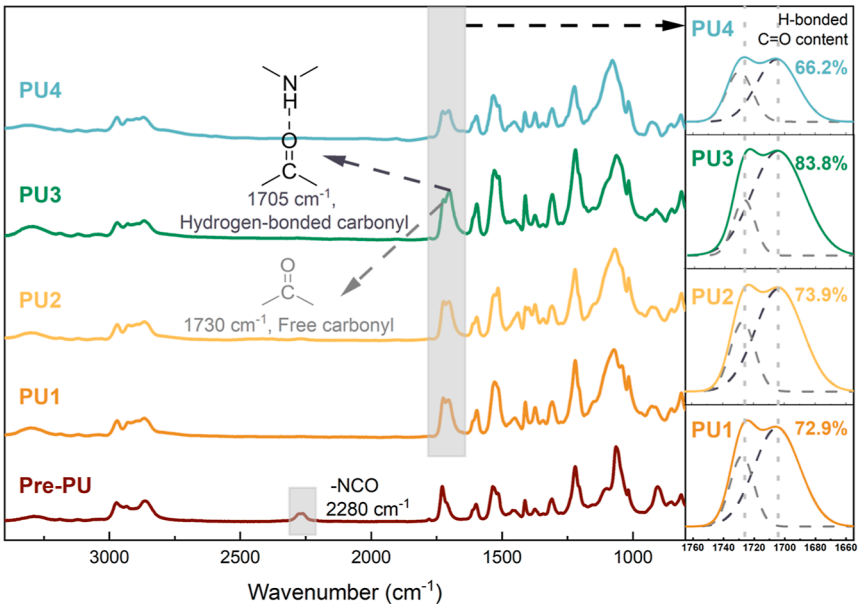

Figure 2. FTIR spectra of PU samples and the deconvolution peaks of the C═O regions.

the reaction was initiated by dripping BDO into the flask for 2 h. The solution was then cast into a Teflon mold with covers and evaporated at 70 °C for 24 h to obtain a thin film with a typical thickness of 500 μm. Anhydrous tetrahydrofuran (THF) was used as the solvent to aid viscosity regulation in the two-step process. For all samples, the ratio of isocyanate groups to total hydroxyl groups, r = [NCO]/[OH], was kept at unity to obtain fully end-linked linear chains. Meanwhile, samples with different HS ratios were obtained by controlling the number of chain extenders. The synthesis route of PUs and the chemical composition of the designed PUs are listed in Figure 1 and Table 1, respectively. Gel permeation chromatography (GPC, Agilent) was used to characterize the molecular weight and molecular weight distribution of the PU samples. The samples were dissolved in a THF solvent. The polymer solution flowed through a column containing different pore sizes with a mobile phase flow rate of 1.0 mL/min. The molecular weight distribution of the designed PUs and their number-average molecular weight (M_n) and weight-average molecular weight (M_w) are shown in Figure S1 and Table S1, separately. The M_n and M_w values of the synthesized PUs increase with the increase of the HS content. The results are in accord with the expectations since the utilization of more chain extenders means that more repeating urethane units are incorporated into the PU backbone while keeping the same isocyanate index constant.

Characterization. A FTIR spectrometer (Thermo Fisher Nicolet iS10, USA) was used to characterize the chemical composition of PUs between 650 and 4000 cm^{-1} with a resolution of 2 cm^{-1}. The microphase separation structure of PUs was carried out with AFM (Bruker Dimension Icon) in the peak force mode. PU samples with a thickness of 200 nm were prepared by drop-coating for AFM tests.

DC volume resistivity was measured with a digital high-resolution electrometer (Keithley 2635B, USA) equipped with a standard three-electrode system. The measurements were performed on the samples with a thickness of around 500 μm and with a 1−15 kV/mm DC electrical field applied. The ambient temperature was controlled at 23 °C using an incubator. This procedure was repeated for different samples to obtain consistent data. No significant difference was found between the primary and repeated experiments. DC electric breakdown tests were performed using a dielectric strength tester (HT-50, Guilin Electrical Equipment Scientific Research Institute, China) on film samples with a thickness of around 500 μm at 23 °C. The samples were sandwiched between two 10 mm ball electrodes and immersed in silicone oil to prevent surface flashover. An increasing ramp voltage, increased at a rate of 1 kV/s, was applied across each of the samples until dielectric breakdown was achieved. For each sample, 15 different points were tested, and the test data were processed using a two-parameter Weibull statistical distribution according to IEEE Std 930-2004.

The thermal stimulation current (TSC) theory can use thermal stimulation to distinguish the charged particles of different activation energies in the dielectric, and the obtained TSC peaks reflect the charge behavior of the dielectric.[31] The sample was polarized under 1.5 kV/mm at 25 °C for 30 min, cooled to −50 °C at a rate of 10 K/min, and then heated to 60 °C at a rate of 5 K/min. During the heating process, the depolarization current of the material was measured by an electrometer (Keithley 6517b). Differential scanning calorimetry (DSC, TA Instruments Q2000, USA) tests were carried out to assist in the analysis on distinguishing the different depolarization current peaks and obtaining the thermal properties of PUs. Samples for DSC tests were prepared by cutting 5 mg of the prepared PUs into hermetically sealed aluminum pans. All samples were allowed to attain isothermal equilibrium at 30 °C for 10 min and then heated to 150 °C to erase the thermal history of the prepared

https://doi.org/10.1021/acsapm.3c01155
ACS Appl. Polym. Mater. 2023, 5, 7132−7143

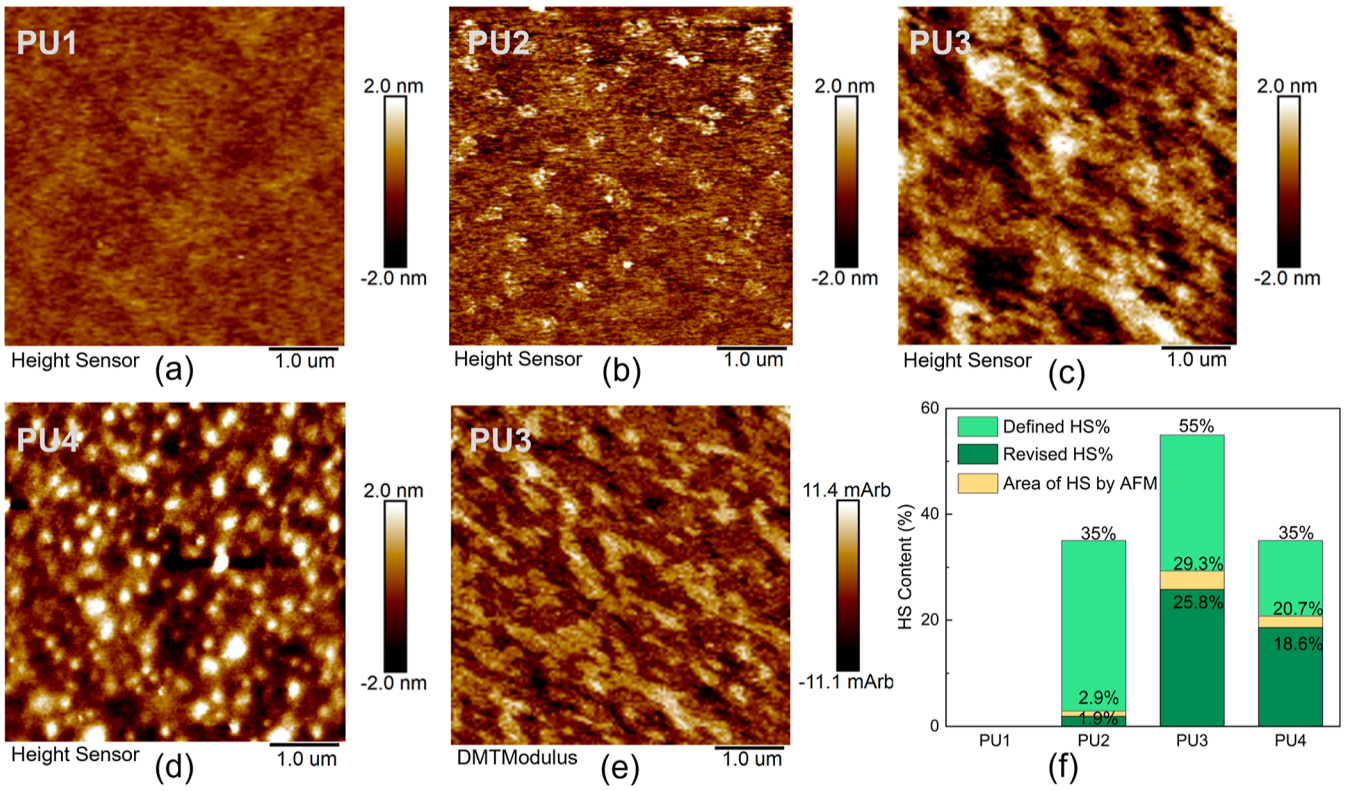

Figure 3. Height image of (a) PU1, (b) PU2, (c) PU3, and (d) PU4 and the corresponding DMT modulus map of (e) PU3 as obtained by AFM. (f) HS contents of PU samples as obtained by different calculating approaches.

samples before collecting data. The response was measured at a heating/cooling rate of 5 °C/min through cooling to −50 °C and heating back to 200 °C. The density functional theory method calculations with the b3lyp/6-31g(d) base are carried out to understand the electron-transfer mechanism in the PU molecular chain in the quantum chemical software Gaussian 09 (Gaussian, Inc.).[32]

The self-healing performance of the prepared PUs was verified by the deliberate introduction of electrical damage. A needle-plate electrode system was used to initiate electrical trees, and the distance between electrodes was 2 mm. The sample was immersed in transformer oil to prevent a surface flashover. An AC voltage of 15 kV/50 Hz was applied for 60 min. After that, the samples were placed in suitable conditions for heating. A multichannel digital partial discharge (PD) analyzer (TWPD-2E, Baoding Tianwei, China) was used to detect the maximum apparent discharge amplitude (Q_m) under an applied voltage of 3 kV at different stages of tree formation and healing to characterize the degree of electrical aging. The 3D topographic features of the electrical tree channel before and after healing were performed on a 3D X-ray micro-CT (3D-CT, Xradia micro-XCT-500, Carl Zeiss XRM, Germany). The samples were mounted on the holder with an Al tube as the adapter and rotated horizontally, pausing at discrete angles to collect 2D projection images, which were then combined to produce a 3D reconstruction of the sample's volume data set. Meanwhile, the in situ self-healing process was monitored by a 2D optical microscope (Nikon DS-Ri2). The micromorphology of electrical tree channels before and after healing was observed by using a scanning electron microscope (SEM, Hitachi SU8010).

A small-scale in situ FTIR between 1640 and 1780 cm^{-1} was used to scan the state of the hydrogen bonding network of PU samples at different temperature points. Dynamic mechanical analysis (DMA, Q800 TA Instrument) was performed for tensile tests of PU samples at a heating rate of 2 °C/min from −50 to 100 °C. Conformational entropy of different molecular architecture was used to evaluate the shape memory effect of PUs.[33]

RESULTS AND DISCUSSION

Hydrogen Bonding Cross-Linking Network of PUs. The chemical composition of PU samples is revealed in the FTIR spectra shown in Figure 2. After curing, the −NCO absorbance peak around 2280 cm^{-1} disappeared, which confirmed that the synthesis reaction of PUs was completed. Hydrogen bonding between the secondary amine group (−NH) and the carbonyl group (C═O) is the intrinsic driving force for the phase separation of PUs, which is important for the self-healing performance.[34] The hydrogen bonding interaction makes the carbonyl bond length elongated and results in the reduction of the stretching vibration frequency.[35] Hence, mathematical deconvolution of the carbonyl stretch peak around 1740 cm^{-1} can be used to divide the free and hydrogen carbonyl, while the stretching peak at lower wavenumber belongs to H-bonding carbonyl.[36] As shown in the partially enlarged drawing of Figure 2, a hydrogen-bonded carbonyl stretching peak is found at 1705 cm^{-1}, which proved the structure of hydrogen bond cross-linking between different chain segments of PU samples. The addition of chain extender will not significantly affect the content of H-bonding carbonyl of PUs, when using the same formulation of PPG and MDI. Even if there are no so-called HS in PU1, hydrogen bonds might still be formed between nonadjacent −NH and C═O groups in SS. The hydrogen bond cross-linking degree of PUs increases with the increase of the HS content, where the H-bonding C═O content increased from 73.9% of PU2 to 83.8% of PU3. Yet, a longer molecular chain of PPG will lead to a lower degree of hydrogen bond cross-linking of PUs with the same HS content.

Microphase Separating Structure of PUs. AFM has been widely used to investigate the nanoscale morphology of

https://doi.org/10.1021/acsapm.3c01155
ACS Appl. Polym. Mater. 2023, 5, 7132−7143

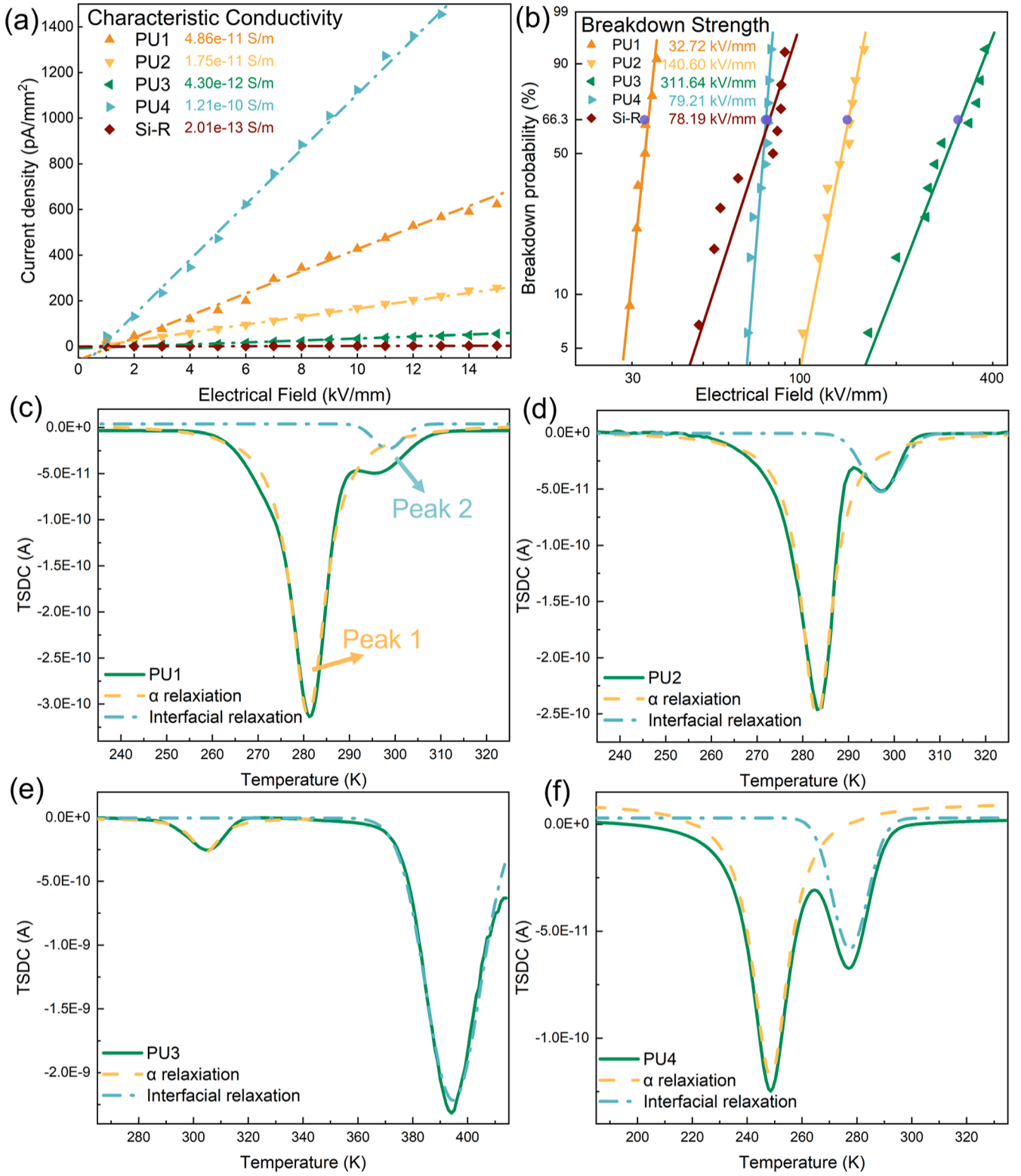

Figure 4. (a) DC conductivity properties of the designed PUs. (b) Weibull characteristic DC breakdown strength of the designed PUs. TSDC spectrum and peak fitting results of (c) PU1, (d) PU2, (e) PU3, and (f) PU4.

the microphase domain in PUs.[37,38] The height images of PU1, PU2, PU3, and PU4 as obtained by AFM are presented in Figure 3a–d, separately. The bright speckles in these images, the "bumps" of the surface, are generally considered as a key feature formed by the orderly stacking and higher modulus of the HS regions.[39] The corresponding modulus mapping of PU3 with the largest bright region in the height image is also measured at the same position, as shown in Figure 3e. DMT modulus is the Young's modulus (the rigidity modulus of an ideal elastic isotropic material) which is calculated by using the load force plus adhesion on the AFM peaking force mode. There is a high consistency between the bright speckles in the

https://doi.org/10.1021/acsapm.3c01155
ACS Appl. Polym. Mater. 2023, 5, 7132−7143

height image and the high-modulus area in the modulus mapping. Hence, the "bumps" in the height graph can be identified as the aggregating domain of HS. Although the defined HS % (wt % of HSs) is revealed in Table 1, only isocyanates that react with chain extenders can form the so-called HS. A revised HS % is given by multiplying the defined HS % by the percentage of the number of moles of the chain extender by all of the polyols in the synthesis. Additionally, the region with height above 1 nm in the AFM image is allocated to the HS domain, and the actual HS % is defined as the area percentage of HS, as presented in Figure 3f. The actual HS % is very close to the revised HS %. The actual HS % of PU1 is 0 due to the absence of a chain extender. Comparing the AFM images of PU2 and PU3, the hard phase transforms from the dotted distribution of PU2 to the large area of banded distribution of PU3 in the continuous distributed soft phase, while the actual HS % also increased from 2.9 to 25.8%. The actual HS % of PU4 is 20.7%, and its HS domain is significantly increased, but the hard phase has not aggregated to form a banded distribution.

Electrical Performance. DC conductivity properties and DC breakdown strength are two significant parameters used for evaluating the electrical properties of dielectric polymers. For a more intuitive comparison, the electrical performance of a common engineering dielectric elastomer (silicone rubber, Si-R, Wacker R230) was also tested. Comparing the conductivity results of PU1−PU3, as shown in Figure 4a, the HS % is the critical factor limiting the conductivity of PUs, which decreases as the HS % increases, when the same PPG and MDI are used. It is noticeable that the presence of a longer SS significantly lifts the conductivity of PUs. The conductivity of PU4 is an order of magnitude higher than that of PU2, at the same defined HS %. Although the conductivity of Si-R is generally lower than that of PUs, the opposite results appear in the DC breakdown tests, as shown in Figure 4b. The breakdown strength of Si-R is 78.19 kV/mm, which is higher than that of PU1 at 32.72 kV/mm. The absence of the HS constructed from isocyanate and short-chain diols results in a breakdown strength of PU1 that is much lower than those of other PUs. The dielectric strength of PUs with a microphase separating structure is higher than that of Si-R, in which PU2 is 140.60 kV/mm and PU3 is 311.64 kV/mm. Dielectric breakdown is a complex process affected by the coupling of electronic avalanches, thermal effects, and mechanical effects.[40] The microphase structure of PUs can effectively prevent the development of breakdown. PU2 and PU3 with excellent dielectric strength are selected to verify their self-healing performance under electrical damage, in consideration of the electrical behaviors of PUs.

Relaxation Behavior of PUs Obtained by Thermal Stimulation Depolarization Current. The thermal stimulation depolarization current (TSDC) method has been widely used to evaluate various relaxation behaviors and reveal its microparameters in solid dielectrics.[41,42] During the heating measurement process, the frozen charges in the material are excited to form depolarization current at different temperatures according to their different activation energy.[43] However, since the measured TSDC curve is often coupled with multiple current peaks, it is necessary to define and analyze different relaxation behaviors by using reasonable peak fitting methods.[31] Based on the DSC results (Figure S2), Peak 1 comes from the α relaxation process near the glass-transition temperature of PUs. Peak 2 is generally considered to be a Maxwell−Wagner−Sillars (MWS) interfacial relaxation that exists in the interface between the SS and HS in the microphase-separated PUs.[23,44] To better study the different relaxations from the TSDC curves, we fitted the peaks in each curve using two Gaussian functions. The original TSDC curve and fitted peaks are presented in Figure 4c−f.

Each discrete current peak can be described by the first-order kinetics equation of TSDC,[45] in which case the corresponding activation energy and charge density can be obtained from any three points on the peaks (eqs S1−S3). The calculation results of the quantity of charge and activation energy corresponding to each relaxation type are listed in Table 2. The TSDC curves of PU1 and PU2 are very similar

Table 2. Calculation Results of Charge and Activation Energy in Different Relaxation Behaviors

sample code	relaxation peak	charge (nC)	ratio of total charge (%)	activation energy (eV)
PU1	α relaxation	55.14	95.6	1.29
	interfacial relaxation	2.55	4.4	1.63
PU2	α relaxation	39.96	86.3	1.48
	interfacial relaxation	6.32	13.7	1.79
PU3	α relaxation	63.36	8.8	1.80
	interfacial relaxation	658.8	91.2	1.82
PU4	α relaxation	38.63	76.7	0.90
	interfacial relaxation	11.76	23.3	1.39

due to their similar synthetic formulations. The difference is that there are no HS formed by the reaction of BDO and isocyanate in PU1, which leads to a very low proportion of charge contribution from interface relaxation, only 4.4%. In contrast, the microphase-separated structure of PU2 brings an obvious interface polarization effect, while some traps with deeper energy levels are introduced into PU2. The activation energies of α relaxation and interface relaxation in PU2 are increased to 1.48 and 1.79 eV, respectively, with the proportion of interface relaxation charge being 6.32%. With the further growth of the HS content, the HS in PU3 is reversed into a continuous phase, and the degree of phase separation is further increased. The energy level of α relaxation in PU3 increases to 1.8 eV, but the proportion of charge decreases to 8.8%. Although the activation energy of interface relaxation in PU3 has not been significantly improved, the proportion of its charge has surged to 91.2%. Due to the use of longer PPG chain segments, the glass-transition temperature of PU4 is reduced, and the activation energies of α relaxation and interface relaxation are decreased. The lowest activation energy of α-relaxation in the continuous SS phase of PU4 is an important reason for its highest conductivity. However, it is worth noting that PU4 still has a significant interface polarization effect, with an interface charge proportion of 23.3%, which is higher than that of 13.7% of PU2 and 4.4% of PU1. Due to the interface polarization behavior between the SS and HS in the phase-separated PU, some traps with deeper energy levels than the activation energy of their main relaxation will be introduced into PUs. The depth and density of traps together affect the macroscopic insulating properties of PUs. The activation energies for α relaxation and interfacial relaxation of PUs composed of longer, more flexible polyol

https://doi.org/10.1021/acsapm.3c01155
ACS Appl. Polym. Mater. 2023, 5, 7132−7143

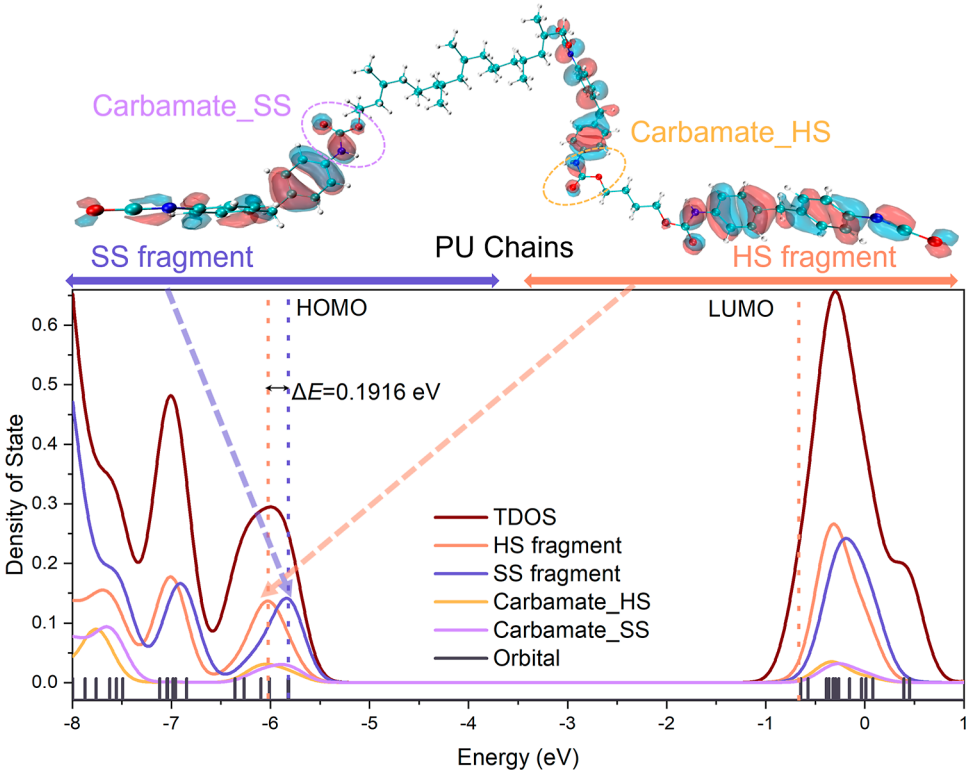

Figure 5. Electron density distribution of the optimized molecular structure of PU repeating units and its molecular orbitals, including the TDOS and partial molecular fragments DOS.

chains are lower than those of PUs composed of short-chain polyols. With the increase of phase separation degree, the charge density of deeper traps also enhances. Traps with deeper energy levels are usually considered unfavorable for charge transport in polymer dielectrics.[46] The TSDC results explain well from the perspective of dielectric relaxation behavior why PU2 and PU3 have lower electrical conductivities and robust dielectric strength.

Quantum Chemical Calculations on Typical PU Chains. To understand the electronic structure of PU molecules and their potential impact on electrical properties, a repeating unit of PU2 segments (Figure S3) was constructed in the first-principles DFT model, where SS fragments composed of PPG (MW = 400) and MDI and HS fragments composed of BDO and MDI assemble the PU segment. The optimized conformation of the typical PU unit is shown in Figure 5, and the total density of states (TDOS) of the molecular orbitals and the partial density of states (DOS) (PDOS) of different molecular fragments were extracted at the same time. The energy level of the highest occupied molecular orbital (HOMO) of the PU unit is −5.8382 eV. It can be seen from Figure 5 that the main contribution to HOMO comes from the carbamate generated by the reaction between PPG/MDI on SS fragments. The carbamate group generated by BDO and MDI on the HS fragments is the main contributor to the HOMO − 1 orbital, whose orbital energy level is −6.0298 eV, and the energy gap between this and HOMO is 0.1916 eV. In solid band theory, HOMO is considered to be the energy level most likely to be excited by heat or electric field to form conduction current across the bandgap barrier.[47] However, there is an energy barrier of 0.1916 eV between the SS and HS of phase-separated PUs, which formed "walls" that hinder charge transportation along the PU chain, thereby enhancing the insulation performance of the materials.

Self-Healing Performance of PUs under Electrical Damage. Figure 6 visually shows the self-healing capability of PU2 against electrical damage. PD in polymers is thought to be a major origin of electrical damage, and the size of the dendritic damage is positively correlated with the maximum apparent discharge magnitude (Q_m).[10] With the increase of aging time, the area of the electrical damage increases, and the Q_m of PU2 also reaches a peak value of 974.34 pC. Within 30 min after voltage withdrawal, it can be obviously observed from the 2D image as obtained by an optical microscope that the terminal dendritic channels of PU2 were closed at room temperature due to the shape memory effect, while the Q_m drops to 724.21 pC. The shape memory effect of PU stems from the ability of its SSs to maintain deformation-induced segment orientation by vitrification transition, i.e., to recover their original shape after deformation.[48,49] Therefore, for slight damage of PU2, such as terminal discharge channels or small branches of electric trees, it can be completely or mostly healed within a short time (30 min) without any external stimulation. Further thermal treatment is required to promote recross-linking of the reversible hydrogen bond network for healing those major dendritic channels. There are only a few main branches in PU2 observed by an optical microscope after 24 h of heating healing at 50 °C, and the Q_m level also dropped back to the initial level. After 48 h, the healing of PU2 is close to saturation. Most of the hollow channels of PU2 were healed, and the PD property was fully restored. Besides that, the SEM images of the cross sections of the samples reflect that the holes and channels around the damaged region in PU2 are refilled after heat-healing. The 3D morphological feature of PU2 was characterized by 3D-CT with a voxel length of 0.6

https://doi.org/10.1021/acsapm.3c01155
ACS Appl. Polym. Mater. 2023, 5, 7132−7143

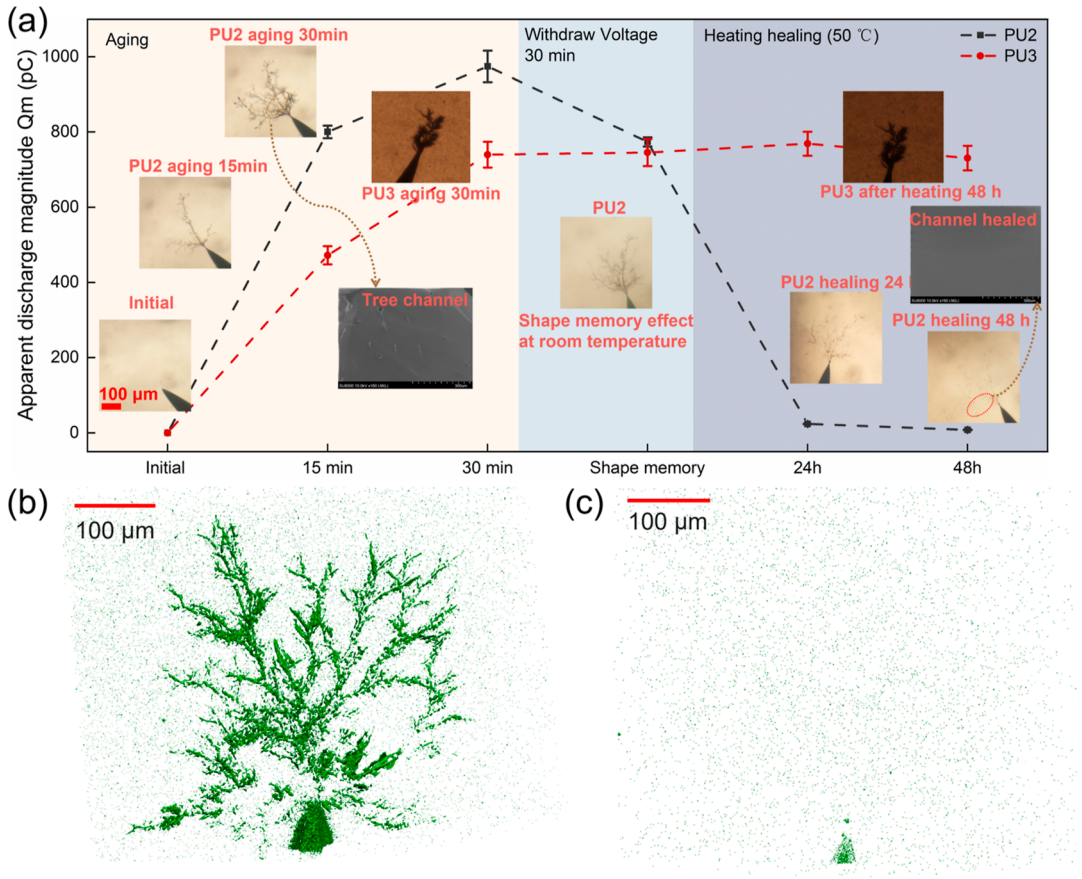

Figure 6. (a) Maximum apparent discharge magnitude (Q_m) of PU2 and PU3 that was electrically aged for 30 min and then heated to heal for 48 h, where the Q_m value and the max−min error bars were measured in the PD tests, and the 2D optical images were taken from the PU samples at different aging/healing stages. There are two SEM images as obtained from two different aged and healed samples since the sample preparation for cross-sectional SEM is destructive. The 3D reconstruction image of electrical damage in PU2 by 3D-CT. (b) Electrically aging for 30 min. (c) 50 °C healing for 48 h.

μm. Figure 6 shows PU2 samples after aging for 30 min and healing for 48 h, which is consistent with the samples observed by an optical microscope in Figure 6. The 3D-CT results confirmed that the dendritic hollow channels in PU2 are completely repaired. PU3 did not exhibit the expected self-healing capabilities, including recovery of electrical properties and healing of channels, which may be related to the low contents of reversible SS phase. For macroscopic mechanical damage, PU2 also shows a good self-healing capability, as indicated in Figure S4. The self-healing efficiency of PU2 evaluated by conductivity or tensile strength is up to 95%.

Reversibility of Hydrogen Bonding Networks. In situ FTIR spectroscopy is the usual methodology for investigating the status of hydrogen bonding at various temperatures.[50] Two thermal cycles were conducted in PU2 and PU3, where FTIR is measured every 10 °C in the heating process. Based on the previous study on PU's FTIR spectroscopy, the carbonyl region from 1780 to 1640 cm^{-1} was mainly demonstrated, as shown in Figure 7. The maximum absorbances of each curve were normalized to 1. The content of hydrogen bonding carbonyl of PU2 decreases when the temperature was above 50 °C, and the hydrogen bonding cross-linking for the PU network is weakened. The content of hydrogen bonding carbonyl of PU2 returns to the initial level when the temperature is reduced to 30 °C. The hydrogen bonding cross-linking network of PU2 shows excellent reversibility in two thermal cycles from 30 to 70 °C, while for PU3, the recross-linking of hydrogen bonds can only occur above 100 °C.

Shape Memory Effects Evaluated by Conformational Entropy. Shape recovery in shape memory PUs is driven by the recuperation of conformational entropy following deformation, which can be fundamentally described in terms of thermodynamics and statistical mechanics.[51] A single DMA experiment allows us to quantify the shape memory effect in terms of stored and released energy densities and their relationship with the shape memory efficiency.[52] The DMA outputs of PU2 and PU3 are illustrated in Figure 7c−f. As the temperature increases from −60 to 110 °C, PU softens while it transitions through the glassy, glass transition, and rubbery plateau regions of viscoelasticity. The glass-transition temperatures (T_g) of PU2 and PU3 are 15.4 and 42.2 °C, respectively. The strain (ε) increases at the onset of the glass transition and subsequently retracts back as the temperature increases. The length increase is considered as a result of the molecular architecture and viscoelastic changes of a polymer, while the length retraction is attributed to conformational entropy and the shape memory effect. This behavior can be quantified in terms of stored entropic energy density (ΔS_S, kJ/m^3), which combines the stress and the strain aspects of shape recovery. ΔS_S is expected to be proportional to the product of the maximum strain (ε_{max}) and stress at maximum strain ($\sigma_{\varepsilon max}$) and is expressed as[33]

https://doi.org/10.1021/acsapm.3c01155
ACS Appl. Polym. Mater. 2023, 5, 7132−7143

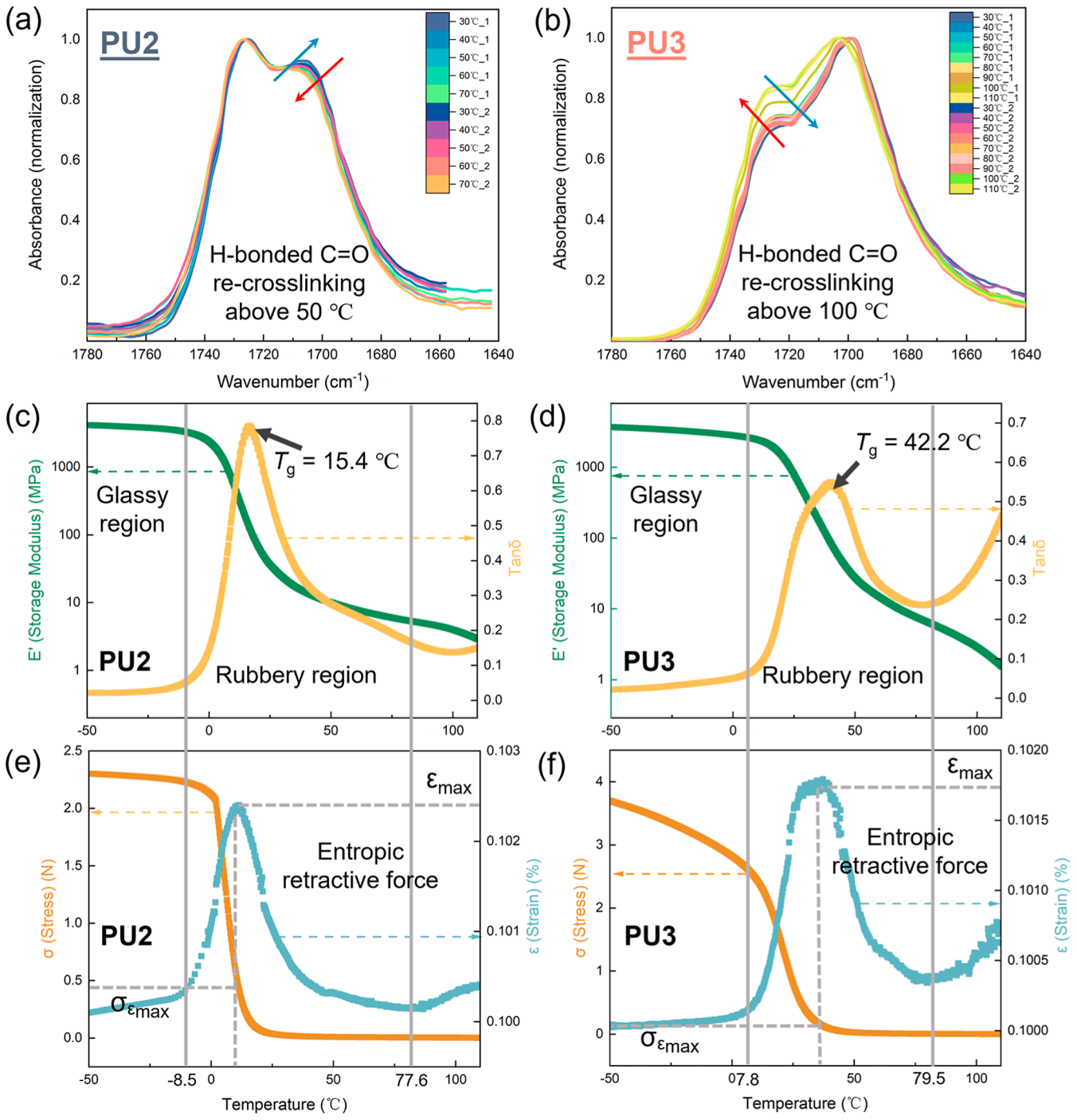

Figure 7. In situ FTIR results at 30−70 °C for PU2 (a) and 30−110 °C for PU3 (b), with a heating rate of 5 °C/min and a hold time of 10 min per point. The trajectory in heating and cooling is indicated by the red and blue arrows, respectively. (c,d) Storage modulus (E') and loss factor (tan δ) of PU2 and PU3 plotted as a function of temperature. (e,f) Stress (σ) and strain (ε) of PU2 and PU3 plotted as a function of temperature as obtained by DMA.

$$\Delta S_s = 5.2819 \times \varepsilon_{max} \times \sigma_{\varepsilon_{max}} \quad (1)$$

The calculated stored entropic energy densities of PU2 and PU3 are 41.13 and 14.18 kJ/m^3, separately, thus indicating that PU2 has more efficient shape memory capability in the rubbery plateau region. The shape recovery ratio (R_r) and shape fixing ratio (R_f) of PU2 and PU3 were also measured by thermomechanical cycles, as shown in Figure S5.

So far, we have a clear and comprehensive understanding of the self-healing behavior of PUs to electrical damage. When the discharge channel is generated, the terminal microcracks will actively close due to the shape memory effect driven by high conformation entropy from the phase separation structure of PU2, preventing further deterioration of the electrical properties. Recross-linking of hydrogen bonding networks occurs under an external stimulus of 50 °C to achieve complete healing of electrical damaged area, while restoring its electrical properties. Figure 8 exhibits the self-healing mechanism in PUs. For PU3, the HS domain has become a continuous phase at 55% HS, which severely restricts the flow of SS, thereby

https://doi.org/10.1021/acsapm.3c01155
ACS Appl. Polym. Mater. 2023, 5, 7132−7143

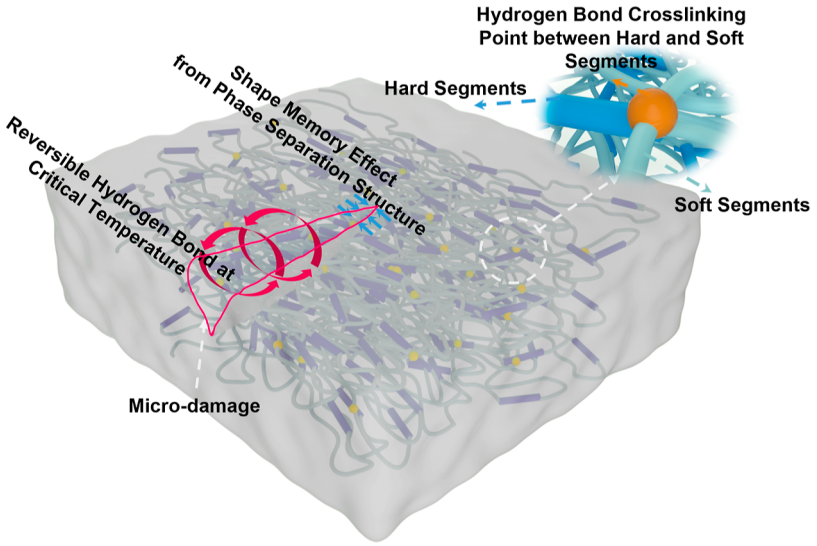

Figure 8. Schematic of self-healing mechanisms in PUs utilizing hydrogen bonding networks and the shape memory effect.

resulting in an inefficient shape memory capability and a temperature of up to 100 °C to achieve the recombination of hydrogen bonds, thus seriously detrimental to self-healing.

CONCLUSIONS

A self-healing PU elastomer with robust dielectric strength utilizing hydrogen bonding cross-linking networks with the shape memory effect was designed and implemented. The hydrogen bonding cross-linking status and the microphase separating morphology of the designed PUs were obtained by deconvoluted FTIR and AFM. PU2 and PU3 constructed with microphase separating structures with high dielectric strength were confirmed by their DC conductivity and breakdown properties. The structure−property relationship of microphase-separated PUs was characterized from two aspects: dielectric relaxation behavior and quantum chemical calculation. The energy barrier at the interface between the soft and hard phases is the critical factor in improving the insulation performance of PUs. Observations from 3D-CT and optical microscopy show that PU2 can fully heal the electrically damaged area at 50 °C while the maximum apparent discharge magnitude drops back to the initial level. The calculation results from DMA show that PU2 has a high conformational entropy, which is helpful in achieving an efficient shape memory effect to heal the terminal dendritic channels of PU2 without the external stimuli. Meanwhile, the reversibility of the hydrogen bonding cross-linking networks of PU2 was verified by variable temperature FTIR. The efficient self-healing capability of PU2 is attributed to its shape memory effect driven by high conformational entropy and the reversibility of hydrogen bonds. The developed self-healing block PU with excellent dielectric strength offers opportunities for reliable applications of self-healing dielectrics in electrical and electronic equipment.

ASSOCIATED CONTENT

Supporting Information

The Supporting Information is available free of charge at https://pubs.acs.org/doi/10.1021/acsapm.3c01155.

Molecular weight distribution obtained by GPC of different PU samples; number-average molecular weight and weight-average molecular weight of designed PUs; DSC thermogram and glass-transition temperatures of the designed PUs; tensile strength and elongation at break of the designed PUs; calculation equations for activation and energy density based on the TSDC curve; molecular structure of PU's repeating unit for DFT calculation; self-healing properties of PU2 under mechanical damage evaluated by conductivity and tensile strength; and shape recovery ratio and shape fixing ratio of PU2 and PU3 (PDF)

AUTHOR INFORMATION

Corresponding Authors

Tian Tan − *Department of Electronic and Electrical Engineering, University of Strathclyde, Glasgow G1 1XW, U.K.*; orcid.org/0000-0002-7135-0943; Email: tian.tan@strath.ac.uk

Qi Li − *State Key Laboratory of Power System, Department of Electrical Engineering, Tsinghua University, Beijing 100084, China*; orcid.org/0000-0002-8282-4884; Email: qili1020@tsinghua.edu.cn

Jinliang He − *State Key Laboratory of Power System, Department of Electrical Engineering, Tsinghua University, Beijing 100084, China*; orcid.org/0000-0002-4458-5026; Email: hejl@tsinghua.edu.cn

Authors

Wah Hoon Siew − *Department of Electronic and Electrical Engineering, University of Strathclyde, Glasgow G1 1XW, U.K.*

Lu Han − *State Key Laboratory of Power System, Department of Electrical Engineering, Tsinghua University, Beijing 100084, China*; orcid.org/0000-0003-4688-0907

Martin Given − *Department of Electronic and Electrical Engineering, University of Strathclyde, Glasgow G1 1XW, U.K.*; orcid.org/0000-0002-6354-2486

Christina McKendry − *Department of Pure and Applied Chemistry, University of Strathclyde, Glasgow G1 1XW, U.K.*

John Liggat − *Department of Pure and Applied Chemistry, University of Strathclyde, Glasgow G1 1XW, U.K.*

Complete contact information is available at: https://pubs.acs.org/10.1021/acsapm.3c01155

Notes

The authors declare no competing financial interest.

■ ACKNOWLEDGMENTS

The authors acknowledge the support of the National Key R&D Program of China (grant 2018YFE0200100) and the National Natural Science Foundation of China (grant 51921005) and for the support of Strathclyde in providing funding for this collaborative project and additional travel funding to facilitate the cooperation of the PhD Cluster on Novel Insulation Materials in both institutions (University of Strathclyde Strategic Partners Initiative: ISP 2019/20 Award—Project with Tsinghua University).

■ REFERENCES

(1) Liu, Z.; Zhang, F.; Yu, J.; Gao, K.; Ma, W. Research on Key Technologies in ± 1100 KV Ultra-high Voltage DC Transmission. *High Voltage* **2018**, *3* (4), 279−288.
(2) Zeng, F.; Chen, X.; Xiao, G.; Li, H.; Xia, S.; Wang, J. A Bioinspired Ultratough Multifunctional Mica-Based Nanopaper with 3D Aramid Nanofiber Framework as an Electrical Insulating Material. *ACS Nano* **2020**, *14* (1), 611−619.
(3) Zhao, X.; Yang, X.; Gao, L.; Li, Q.; Hu, J.; He, J. Tuning the Potential Distribution of AC Cable Terminals by Stress Cone of Nonlinear Conductivity Material. *IEEE Trans. Dielectr. Electr. Insul.* **2017**, *24* (5), 2686−2693.
(4) Wang, Q.; Chen, X.; Huang, X.; Muhammad, A.; Paramane, A.; Ren, N. Enhanced Field-Dependent Conductivity and Material Properties of Nano-AlN/Micro-SiC/Silicone Elastomer Hybrid Composites for Electric Stress Mitigation in High-Voltage Power Modules. *Nanotechnology* **2022**, *33* (47), 475706.
(5) Chen, X.; Wang, Q.; Huang, X.; Muhammad, A.; Paramane, A.; Ren, N. Enhancement of Electrical Properties by Including Nano-Aluminum Nitride to Micro-Silicon Carbide/Silicone Elastomer Composites for Potential Power Module Packaging Applications. *J. Mater. Sci. Mater. Electron.* **2022**, *33* (23), 18768−18785.
(6) Cherney, E. A. Nanodielectrics Applications — Today and Tomorrow. *IEEE Electr. Insul. Mag.* **2013**, *29* (6), 59−65.
(7) Tanaka, T. Dielectric Nanocomposites with Insulating Properties. *IEEE Trans. Dielectr. Electr. Insul.* **2005**, *12* (5), 914−928.
(8) Wutzel, H.; Jarvid, M.; Bjuggren, J. M.; Johansson, A.; Englund, V.; Gubanski, S.; Andersson, M. R. Thioxanthone Derivatives as Stabilizers against Electrical Breakdown in Cross-Linked Polyethylene for High Voltage Cable Applications. *Polym. Degrad. Stab.* **2015**, *112*, 63−69.
(9) Liu, M.; Liu, Y.; Li, Y.; Zheng, P.; Rui, H. Growth and Partial Discharge Characteristics of Electrical Tree in XLPE under AC-DC Composite Voltage. *IEEE Trans. Dielectr. Electr. Insul.* **2017**, *24* (4), 2282−2290.
(10) Chen, X.; Xu, Y.; Cao, X.; Dodd, S.; Dissado, L. Effect of Tree Channel Conductivity on Electrical Tree Shape and Breakdown in XLPE Cable Insulation Samples. *IEEE Trans. Dielectr. Electr. Insul.* **2011**, *18* (3), 847−860.
(11) Dissado, L. A. Theoretical Basis for the Statistics of Dielectric Breakdown. *J. Phys. D Appl. Phys.* **1990**, *23* (12), 1582−1591.
(12) Huang, X.; Han, L.; Yang, X.; Huang, Z.; Hu, J.; Li, Q.; He, J. Smart Dielectric Materials for Next-Generation Electrical Insulation. *iEnergy* **2022**, *1* (1), 19−49.
(13) Yang, Y.; He, J.; Li, Q.; Gao, L.; Hu, J.; Zeng, R.; Qin, J.; Wang, S. X.; Wang, Q. Self-Healing of Electrical Damage in Polymers Using Superparamagnetic Nanoparticles. *Nat. Nanotechnol.* **2019**, *14* (2), 151−155.
(14) Wang, Y.; Li, Y.; Zhang, Z.; Zhang, Y. Effect of Doping Microcapsules on Typical Electrical Performances of Self-Healing Polyethylene Insulating Composite. *Appl. Sci.* **2019**, *9* (15), 3039.
(15) Gao, L.; Yang, Y.; Xie, J.; Zhang, S.; Hu, J.; Zeng, R.; He, J.; Li, Q.; Wang, Q. Autonomous Self-Healing of Electrical Degradation in Dielectric Polymers Using in Situ Electroluminescence. *Matter* **2020**, *2* (2), 451−463.
(16) Xie, J.; Gao, L.; Hu, J.; Li, Q.; He, J. Self-Healing of Electrical Damage in Thermoset Polymers: Via Anionic Polymerization. *J. Mater. Chem. C* **2020**, *8* (18), 6025−6033.
(17) Xie, J.; Han, L.; Luo, Z.; Li, Q.; He, J. Microcapsule-Based Autonomous Self-Healing of Electrical Damage in Dielectric Polymers Induced by In Situ Generated Radicals. *ACS Appl. Mater. Interfaces* **2023**, *15* (8), 11185−11192.
(18) Wu, D. Y.; Meure, S.; Solomon, D. Self-Healing Polymeric Materials: A Review of Recent Developments. *Prog. Polym. Sci.* **2008**, *33* (5), 479−522.
(19) Menon, A. V.; Madras, G.; Bose, S. Light Weight, Ultrathin, and "Thermally-Clickable" Self-Healing MWNT Patch as Electromagnetic Interference Suppressor. *Chem. Eng. J.* **2019**, *366*, 72−82.
(20) Xie, J.; Yang, M.; Liang, J.; Hu, J.; Li, Q.; He, J. Self-Healing of Internal Damage in Mechanically Robust Polymers Utilizing a Reversibly Convertible Molecular Network. *J. Mater. Chem. A* **2021**, *9* (29), 15975−15984.
(21) Zhou, Y.; Li, L.; Han, Z.; Li, Q.; He, J.; Wang, Q. Self-Healing Polymers for Electronics and Energy Devices. *Chem. Rev.* **2023**, *123* (2), 558−612.
(22) Mokeev, M. V.; Ostanin, S. A.; Saprykina, N. N.; Zuev, V. V.; Menon, A. V.; Madras, G.; Bose, S. Microphase Structure of Polyurethane-Polyurea Copolymers as Revealed by Solid-State NMR: Effect of Molecular Architecture. *Polymer* **2018**, *150*, 72−83.
(23) Heydarnezhad, H. R.; Mohammadi, N.; Arbe, A.; Alegria, A. How Does Microstructural Design Affect the Dynamics and Rheology of Segmented Polyurethanes? *Macromolecules* **2020**, *53* (13), 5381−5398.
(24) Menon, A. V.; Madras, G.; Bose, S. The Journey of Self-Healing and Shape Memory Polyurethanes from Bench to Translational Research. *Polym. Chem.* **2019**, *10*, 4370−4388.
(25) Yuan, C.; Rong, M. Z.; Zhang, M. Q. Self-Healing Polyurethane Elastomer with Thermally Reversible Alkoxyamines as Crosslinkages. *Polymer* **2014**, *55* (7), 1782−1791.
(26) Krol, P. Synthesis Methods, Chemical Structures and Phase Structures of Linear Polyurethanes. Properties and Applications of Linear Polyurethanes in Polyurethane Elastomers, Copolymers and Ionomers. *Prog. Mater. Sci.* **2007**, *52* (6), 915−1015.
(27) Kang, J.; Tok, J. B.-H.; Bao, Z. Self-Healing Soft Electronics. *Nat. Electron.* **2019**, *2* (4), 144−150.
(28) Sánchez-Adsuar, M. Influence of the Composition on the Crystallinity and Adhesion Properties of Thermoplastic Polyurethane Elastomers. *Int. J. Adhes. Adhes.* **2000**, *20* (4), 291−298.
(29) Castagna, A. M.; Fragiadakis, D.; Lee, H.; Choi, T.; Runt, J. The Role of Hard Segment Content on the Molecular Dynamics of Poly(Tetramethylene Oxide)-Based Polyurethane Copolymers. *Macromolecules* **2011**, *44* (19), 7831−7836.
(30) Zhang, M. Q.; Rong, M. Z. Intrinsic Self-Healing of Covalent Polymers through Bond Reconnection towards Strength Restoration. *Polym. Chem.* **2013**, *4* (18), 4878−4884.
(31) Qin, S.; Tu, Y.; Tan, T.; Wang, S.; Yuan, Z.; Wang, C.; Li, L.; Wu, Z. The Effects of γ-Ray on Charging Behaviour Using Polyimide. *J. Phys. D Appl. Phys.* **2018**, *51* (24), 245302.
(32) Lu, T.; Chen, F. Multiwfn: A Multifunctional Wavefunction Analyzer. *J. Comput. Chem.* **2012**, *33* (5), 580−592.
(33) Hornat, C. C.; Yang, Y.; Urban, M. W. Quantitative Predictions of Shape-Memory Effects in Polymers. *Adv. Mater.* **2017**, *29* (7), 1603334−1603338.
(34) Grzelak, A. W.; Boinard, P.; Liggat, J. J. The Influence of Diol Chain Extender on Morphology and Properties of Thermally-Triggered UV-Stable Self-Healing Polyurethane Coatings. *Prog. Org. Coat.* **2018**, *122*, 1−9.
(35) Mishra, A. K.; Chattopadhyay, D. K.; Sreedhar, B.; Raju, K. V. S. N. FT-IR and XPS Studies of Polyurethane-Urea-Imide Coatings. *Prog. Org. Coat.* **2006**, *55* (3), 231−243.

https://doi.org/10.1021/acsapm.3c01155
ACS Appl. Polym. Mater. 2023, 5, 7132−7143

(36) Furukawa, M.; Kojio, K.; Kugumiya, S.; Uchiba, Y.; Mitsui, Y. Microphase Separation of Bulk and Ultrathin Films of Polyurethane Elastomers. *Macromol. Symp.* **2008**, *267* (1), 9−15.
(37) Schön, P.; Bagdi, K.; Molnár, K.; Markus, P.; Pukánszky, B.; Julius Vancso, G. Quantitative Mapping of Elastic Moduli at the Nanoscale in Phase Separated Polyurethanes by AFM. *Eur. Polym. J.* **2011**, *47* (4), 692−698.
(38) Jiang, L.; Wu, J.; Nedolisa, C.; Saiani, A.; Assender, H. E. Phase Separation and Crystallization in High Hard Block Content Polyurethane Thin Films. *Macromolecules* **2015**, *48* (15), 5358−5366.
(39) Imre, B.; Gojzewski, H.; Check, C.; Chartoff, R.; Vancso, G. J. Properties and Phase Structure of Polycaprolactone-Based Segmented Polyurethanes with Varying Hard and Soft Segments: Effects of Processing Conditions. *Macromol. Chem. Phys.* **2018**, *219* (2), 1700214−1700313.
(40) Wang, W.; Li, S. Research Status and Development of Insulation Breakdown in Engineering Solid Dielectrics. *Kexue Tongbao* **2020**, *65* (31), 3461−3474.
(41) Tsonos, C.; Apekis, L.; Zois, C.; Tsonos, G. Microphase Separation in Ion-Containing Polyurethanes Studied by Dielectric Measurements. *Acta Mater.* **2004**, *52* (5), 1319−1326.
(42) Diogo, H. P.; Moura Ramos, J. J. Contribution of the Technique of Thermostimulated Currents for the Elucidation of the Nature of the Johari-Goldstein and Other Secondary Relaxations in the Vitreous State. *IEEE Trans. Dielectr. Electr. Insul.* **2014**, *21* (5), 2301−2309.
(43) Chen, R. Methods for Kinetic Analysis of Thermally Stimulated Processes. *J. Mater. Sci.* **1976**, *11* (8), 1521−1541.
(44) Ortiz-Serna, P.; Carsí, M.; Redondo-Foj, B.; Sanchis, M. J.; Culebras, M.; Gómez, C. M.; Cantarero, A. Thermal and Dielectric Properties of Polycarbonatediol Polyurethane. *J. Appl. Polym. Sci.* **2015**, *132* (22), 1−8.
(45) Kamalov, A. M.; Borisova, M. E. The Influence of Moisture on Charge Relaxation in Modified Polyimide Films. *St. Petersbg. State Polytech. Univ. J.: Phys. Math.* **2016**, *2* (3), 188−192.
(46) Sun, W.; Xu, J.; Song, J.; Chen, Y.; Lv, Z.; Cheng, Y.; Zhang, L. Self-Healing of Electrical Damage in Insulating Robust Epoxy Containing Dynamic Fluorine-Substituted Carbamate Bonds for Green Dielectrics. *Mater. Horiz.* **2023**, *10*, 2542−2553.
(47) Takada, T.; Kikuchi, H.; Miyake, H.; Tanaka, Y.; Yoshida, M.; Hayase, Y. Determination of Charge-Trapping Sites in Saturated and Aromatic Polymers by Quantum Chemical Calculation. *IEEE Trans. Dielectr. Electr. Insul.* **2015**, *22* (2), 1240−1249.
(48) Gunes, I. S.; Cao, F.; Jana, S. C. Evaluation of Nanoparticulate Fillers for Development of Shape Memory Polyurethane Nanocomposites. *Polymer* **2008**, *49* (9), 2223−2234.
(49) Meng, H.; Li, G. A Review of Stimuli-Responsive Shape Memory Polymer Composites. *Polymer* **2013**, *54* (9), 2199−2221.
(50) Li, L.; Yang, G. Variable-Temperature FTIR Studies on Thermal Stability of Hydrogen Bonding in Nylon 6/Mesoporous Silica Nanocomposite. *Polym. Int.* **2009**, *58* (5), 503−510.
(51) Hornat, C. C.; Urban, M. W. Shape Memory Effects in Self-Healing Polymers. *Prog. Polym. Sci.* **2020**, *102*, 101208.
(52) Xie, T. Recent Advances in Polymer Shape Memory. *Polymer* **2011**, *52* (22), 4985−5000.

https://doi.org/10.1021/acsapm.3c01155
ACS Appl. Polym. Mater. 2023, 5, 7132−7143